

Corrosion Behavior of Squeeze Cast Mg Alloy AM60-Based Hybrid Nanocomposite

Xinyu Geng, Luyang Ren, Zixi Sun, Henry Hu, and Xueyuan Nie

Abstract

Micron-sized alumina (Al_2O_3) short fibre and/or nano-sized alumina (Al_2O_3) particles were squeezed cast into Mg AM60 alloy. Two types of 7 vol.% Fibre/AM60, and (7 vol. % Fibre + 3 vol.% nano-particle)/AM60 composites, as well as the unreinforced matrix alloy were prepared. The corrosion behaviors of the composites as well as the unreinforced matrix alloy were investigated by using the potential dynamic polarization test. Compared with the matrix alloy, the introduction of micron-sized alumina fibres decreased the corrosion resistance of Mg alloy AM60 considerably due to the presence of excessive interfaces between the fibre and matrix. The high density of grain boundaries and the absence of noble precipitates such as $\beta\text{-Mg}_{17}\text{Al}_{12}$ phases and Al–Mn intermetallics at the grain boundaries in the composites should be for the reduction in their corrosion resistance. The addition of the nano-sized particles led to almost no further reduction in the corrosion resistance of the composite.

Keywords

Magnesium-based hybrid nanocomposite (MHNC) • Corrosion resistance • Mg alloy • Micron-sized alumina (Al_2O_3) short fibre • Nano-sized alumina (Al_2O_3) particles

Introduction

Magnesium (Mg) based materials have become one of the most significant candidates for structural engineering applications due to their lightweight, high thermal conductivity, and good ductility. In automotive industry, magnesium alloys are widely used for building vehicle components such as instrumental panels, cylinder head covers, intake manifolds, transfer cases and so on. Further expansion of new magnesium-based engineering applications is still on-going owing to the stringent government regulations on auto emissions and weight reduction. Hence, magnesium-based metal matrix composites (MMCs) including fiber-reinforced composites, particle reinforced composites and fiber-particle hybrid reinforced composites are emerging and being investigated for the improvement of mechanical properties of monolithic matrix alloys, including high yield strength, tensile strength, creep resistance, thermal shock resistance and wear resistance [1–6].

In the past few years, magnesium alloy-based hybrid composites are emerging since the combined advantages of different sizes of short fibres, and particles provide a high degree of design freedom, which enable fibres to increase strengths and particles to improve wear resistance [6]. Mondal et al. [7] studied the corrosion behavior of creep resistant AE42 magnesium alloy hybrid composites containing micron-sized Al_2O_3 short fibres and SiC particles. The corrosion rates of different reinforcements combination was evaluated by potential dynamic polarization tests in 5 wt % NaCl solution. Their results showed that the tested composites exhibited much higher corrosion rates as compared to that of the unreinforced alloy. The addition of micron-sized SiC particles increased the corrosion rates of the hybrid composites by over 30%. Zhang et al. [6] pointed out that the introduction of micron-size reinforcements into the hybrid composite adversely affected the plasticity of Mg matrix alloys due to particle or fibre cracking and void formation at reinforcement-matrix interface leading to

X. Geng · L. Ren · Z. Sun · H. Hu (✉) · X. Nie
Department of Mechanical, Automotive and Materials
Engineering, University of Windsor, 401 Sunset Ave, Windsor,
ON N9B 3P4, Canada
e-mail: huh@uwindsor.ca

X. Geng
e-mail: gengx@uwindsor.ca

L. Ren
e-mail: ren11h@uwindsor.ca

Z. Sun
e-mail: sun13h@uwindsor.ca

X. Nie
e-mail: xnie@uwindsor.ca

accelerated failure. Recently, the study by Zhou et al. [8] demonstrated that the replacement of the micron-sized particles with the nanoparticles in the Mg-based hybrid composite effectively recovered the ductility of the composite by almost 120%. However, the introduction of foreign particles and/or fibre could deteriorate the corrosion resistance of magnesium alloys. Research on the corrosion behavior of the MHNC in the open literature is scarce.

In the present work, the microstructures of the monolithic matrix alloy AM60, its micron fibre-only composite and the MHNC were analyzed by the optical (OM) and scanning electron microscopes (SEM) and X-ray energy dispersive spectroscopy (EDS). The corrosion behavior of the monolithic matrix alloy AM60, its micron fibre-only composite and the MHNC were assessed by potentiodynamic polarization tests. The changes of the surface morphologies of the tested matrix alloy and composites were analyzed by electron scanning microscopy, and corrosion products were identified by the (EDS) analyses.

Experimental Procedure

Composites Preparation

Magnesium alloy AM60 with a chemical composition (wt%) of 6.0Al–0.22Zn–0.4Mn–0.1Si–0.01Cu–0.004Fe–0.002Ni–Mg was chosen as matrix alloy. Nano-sized Al₂O₃ ceramic particles with an average particulate size of 100 nm and Al₂O₃ short fibres with an average diameter of 4 µm and length of 50 µm were employed as raw materials for the preparation of hybrid reinforcements since they are relatively inexpensive and possess adequate properties.

During composite fabrication, a hybrid preform was first preheated to 700 °C. Then, molten matrix alloy AM60 at 750 °C infiltrated into the preheated preform under an applied pressure of 90 MPa. The pressure was maintained at the desired level for 30 s.

For fabrication of composites, a preform and squeeze casting process were employed. Two different types of 7 vol.% micron fibre/AM60, and (7 vol.% Fibre + 3 vol.% nano-particle)/AM60 composites were prepared, which were named the fibre-only composite (7FC), and the MHNC-7F3NP, respectively. In the hybrid composite, the short fibres constituted the primary reinforcement phase, and the particles served as the secondary reinforcement phase. For the purpose of comparison, the base alloy AM60 was also squeeze cast. The details of the process for fabricating the composites are given in references 6 and 8.

Electrochemical Experimentation

Electrochemical studies were carried out by using EC-LAB SP-150 electrochemical apparatus with corrosion analysis EC-lab software. A three-electrode cell was set up through assigning the samples as working electrode, Ag/AgCl/sat'd KCl electrode as a reference electrode and a Pt metal electrode as counter-electrode. At the beginning of experiments, samples were held in a salt solution allowing the open circuit potential to settle to a constant value. Potentiodynamic polarization scans were conducted at a rate of 10 mV/s from –0.5 V versus open circuit potential in a more noble direction up to 0.5 V versus the reference electrode. Machined samples were ground with silicon carbide papers with various grades from 280 to 2500 grit and then cleaned in acetone, rinsed with deionized water and dried prior to potentiodynamic polarization. The values of corrosion potential (E_{corr}) and current density (i_{corr}) were determined at the intersection between the anodic and cathodic Tafel slopes, which were extrapolated by the linear parts of the polarization curves.

Analyses of Corrosion Surface

The detailed features of the corroded surfaces were characterized at high magnifications using a FEI Quanta 200 FEG (Tokyo, Japan) scanning electron microscope (SEM) with a maximum resolution of 100 nm in a backscattered (BSE) mode/1 µm in X-ray diffraction mapping mode, and maximum useful magnification of 30,000. The corroded surfaces of the unreinforced alloy AM60, and the 7FC and MHNC-7F3NP composites were analyzed by the SEM in secondary electron (SE) mode to ascertain their corrosion mechanisms. Energy dispersive X-ray (EDS) analyses were used to define the elements distribution.

Results and Discussion

Electrochemical Tests

Figure 1 shows the polarization curves of the as-cast unreinforced alloy AM60, and 7FC and MHNC composites. Potentiodynamic polarization curves, measured in 3.5 wt% NaCl solution, were similar for the three tested materials. A summary of the results of potentiodynamic corrosion tests was given in Table 1. The corrosion potentials were in the range from –1.417 to –1.441 V (SCE), typical of

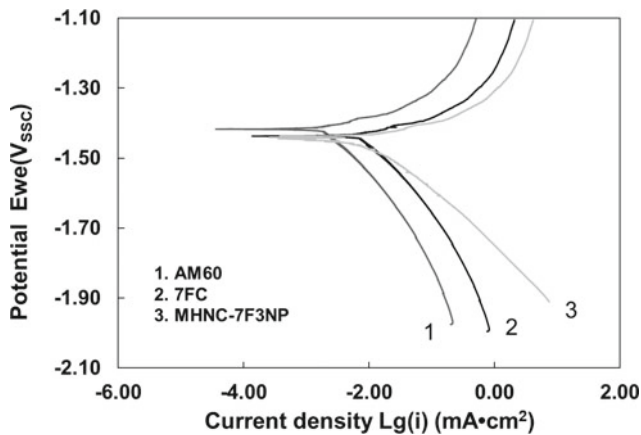


Fig. 1 Polarization curves of the as-cast AM60, 7FC and MHNC-7F3NP composites

magnesium alloys. The curves indicated film breakdown at potentials immediately above the corrosion potential with characteristically low apparent Tafel slopes of about 52.9–29.1 mV decade. At high current densities, the curves were affected by a potential drop due to the solution resistance, and on the cathodic side by the additional resistance due to the formation of hydrogen bubbles. At the end of the tests, the electrodes were covered by a black layer of corrosion products. The color of the products was changed to white after they dried.

Figure 2 displays the corrosion current densities and potentials of the as-cast AM60, and the 7FC and MHNC-7F3NP composites based on the data extracted from Fig. 1. Among the three tested materials, the unreinforced alloy AM60 (Curve 1) had a negative corrosion potential (−1.417 V), which was the highest, while the value of its corrosion current density ($4.71 \mu\text{A}/\text{cm}^2$) was the lowest. Compared to that of the AM60, the polarization curve of the 7FC composite (Curve 2) was shifted to the right and downward. The value of the corrosion potential of the 7FC composite was more negative than that of the AM60 alloy, although the 7FC composite had a corrosion current density higher than that of the AM60 alloy. The polarization curve of the MHNC-7F3NP composite (Curve 3) exhibited a shift to the left and downward in comparison with that of the FC. The MHNC-7F3NP composite possessed a slightly lower corrosion potential and higher density than that of the 7FC.

The corrosion potentials, corrosion current density, and anodic/cathodic Tafel slopes (anodic: β_a and cathodic: β_c) were derived from the test data. Based on the approximate linear polarization at the corrosion potential (E_{corr}), polarization resistance (R_p) values were determined by the relationship [9]:

$$R_p = \frac{\beta_a * \beta_c}{2.3 * i_{\text{corr}} * (\beta_a + \beta_c)} \quad (1)$$

where i_{corr} is the corrosion current density. The data in Table 1 denoted that the corrosion resistance of the AM60 alloy ($4.07 \text{ k}\Omega \text{ cm}^2$) was decreased by the introduction of micron-sized fibres and nano-sized particles. The 7FC composite possessed a high corrosion current density, which was 20% higher than that of the matrix AM60 alloy. The corrosion resistance of the 7FC composite ($2.08 \text{ k}\Omega \text{ cm}^2$) was only a half of that of the matrix alloy. The addition of the micron-sized fibres as reinforcement significantly reduced the corrosion resistance of the matrix alloy AM60 by almost 50%. The corrosion resistance of the MHNC-7F3NP was $1.88 \text{ k}\Omega \text{ cm}^2$. The presence of the nano-sized particles resulted in a reduction of the corrosion resistance of the 7FC composite from 2.08 to $1.88 \text{ k}\Omega \text{ cm}^2$ by $0.20 \text{ k}\Omega \text{ cm}^2$. This observation indicated that the introduction of the nano-sized particles up to 3 vol.% had almost no effect on the corrosion resistance of the FC composite.

In the Tafel extrapolation method for measuring corrosion rates of Mg-based materials, the corrosion current density, i_{corr} ($\mu\text{A}/\text{cm}^2$) is estimated by Tafel extrapolation of the cathodic branch of the polarisation curve, and the obtained i_{corr} can be linearly related to the average corrosion rate, P_i (mm/year) by the following equation [7, 10, 11]

$$P_i = 0.02285 \times i_{\text{corr}} \quad (2)$$

The calculated P_i values are listed in Table 1. Corrosion rates determined based on Tafel extrapolations demonstrate quantitatively the corrosion nature of various materials, although they are somewhat different from those obtained from weight loss or hydrogen evolution measurement [11]. Figure 3 shows the corrosion rates of the as-cast unreinforced alloy AM60, and 7FC and MHNC composites, which were 0.108, 0.130 and 0.136 mm/year, respectively. The introduction of the micron Al_2O_3 fibres increased the

Table 1 Electrochemical parameters of the unreinforced alloy AM60, and the 7FC and MHNC-7F3NP composites

Materials	β_a (mV/dec)	β_c (mV/dec)	i_{corr} ($\mu\text{A}/\text{cm}^2$)	R_p ($\text{k}\Omega \text{ cm}^2$)	E_{corr} (V)	P_i (mm/year)
AM60	52.9	262.5	4.71	4.07	−1.417	0.108
7FC	31.8	188.7	5.68	2.08	−1.437	0.130
MHNC-7F3NP	29.1	128	5.95	1.88	−1.441	0.136

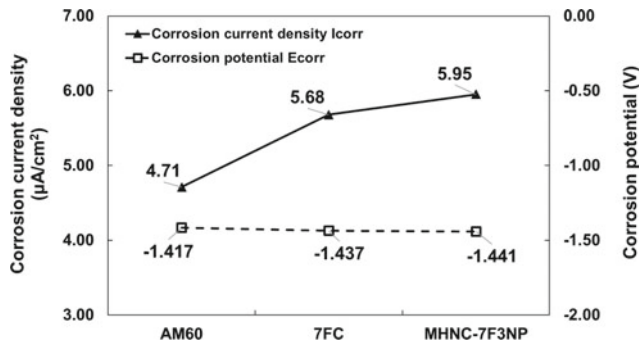


Fig. 2 Corrosion current densities and potentials of the as-cast AM60, and the 7FC and MHNC-7F3NP composites

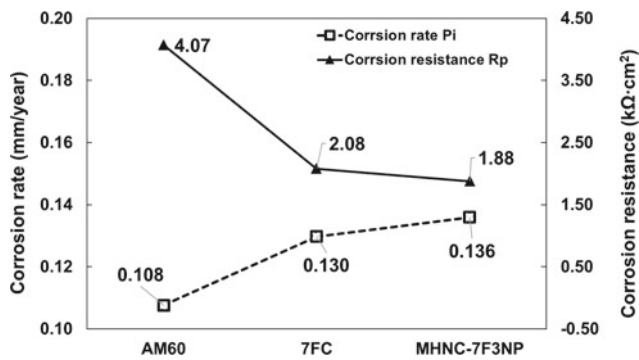


Fig. 3 Corrosion resistances and rates of the as-cast AM60, and the 7FC and MHNC-7F3NP composites

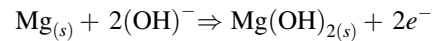
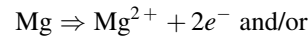
corrosion rate of the matrix alloy by 20%. But, the corrosion rate of the composite rose by only 4% with the further addition of the nano Al_2O_3 particles.

Corroded Surfaces and Corrosion Mechanisms

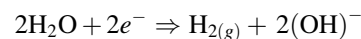
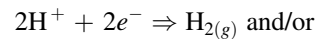
The surface morphologies of the corroded unreinforced alloy AM60, and 7FC and MHNC-7F3NP composites are shown in Fig. 4, after they were immersed in 3.5 wt% NaCl aqueous solution for one hour. The SEM micrograph given in Fig. 4a showed a layer of discontinuous film with corroded products. Figure 5 presents the EDS spectra showing the presence of oxygen and chlorine in the corroded surface of the unreinforced alloy AM60, and 7FC and MHNC-7F3NP composites, which suggested there were $\text{Mg}(\text{OH})_2$ and MgCl in the corroded products. The corrosion behavior of AM60 alloy was significantly influenced by the alloy elements, such as aluminum and manganese. The formation of the surface morphology on the corroded unreinforced alloy AM60 resulted from a combined effect of galvanic

corrosion, and pitting corrosion. The presence of different phases in the microstructure of the unreinforced alloy AM60 should be responsible for these types of corrosion mechanisms. The eutectic $\beta\text{-Mg}_{17}\text{Al}_{12}$ and Al-Mn intermetallic phases in the Mg-Al alloy could serve as cathodic sites, and the primary $\alpha\text{-Mg}$ matrix would be anodic.

Anodic reaction:



Cathodic reaction:



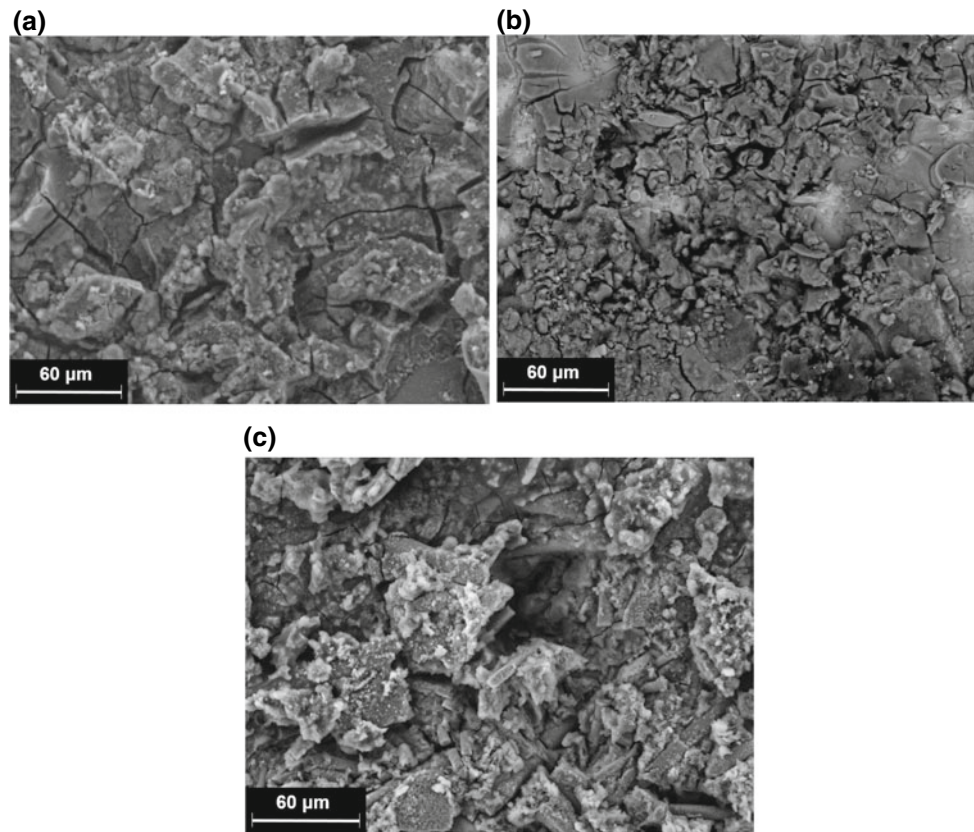
The overall reaction is:



As pointed out by Bakkar and Neubert [12, 13] for magnesium alloy AS41, owing to the high pH region around cathodic area, the passivation surface which contained $\text{MgO}/\text{Mg}(\text{OH})_2$ was formed. The generation of hydrogen and the continuous formation of hydroxide ions kept increasing the pH value and the protective film grew thicker consequently. At the anodic region, the protective film was hardly to be formed due the pH was too low and Mg^{2+} was produced at a high rate from the alloy surface and the pit developed. As a result of maintaining electroneutrality, chloride ions were attracted into the pit. As the corrosion proceeded, the pit grew bigger and deeper and led to the formation of the discontinuous film. Song et al. [14] found that, in magnesium alloy AZ91, the $\beta\text{-Mg}_{17}\text{Al}_{12}$ phase mainly served as a galvanic cathode and accelerated the corrosion process of the primary $\beta\text{-Mg}$ matrix if the volume fraction of $\beta\text{-Mg}_{17}\text{Al}_{12}$ phase was small, although the $\beta\text{-Mg}_{17}\text{Al}_{12}$ phase was very stable in NaCl solutions and was inert to corrosion. Besides the $\beta\text{-Mg}_{17}\text{Al}_{12}$ phase, the most potent cathodes in an Mg-Al alloy are the iron-rich precipitate phases. Heavy metal contamination promoted a general pitting attack.

Figures 4b, c present a SEM micrograph showing the surface morphology of the 7FC and MHNC-7F3NP composites after corrosion testing, which exhibited thick but irregular and loose films. The large and deep corrosion attack can be clearly observed on two composites samples which could be attributed to the crevice attacks of reinforcements.

Fig. 4 SEM micrographs in SE mode showing corroded surfaces of **a** the unreinforced alloy AM60, and the **b** 7FC and **c** MHNC-7F3NP composites



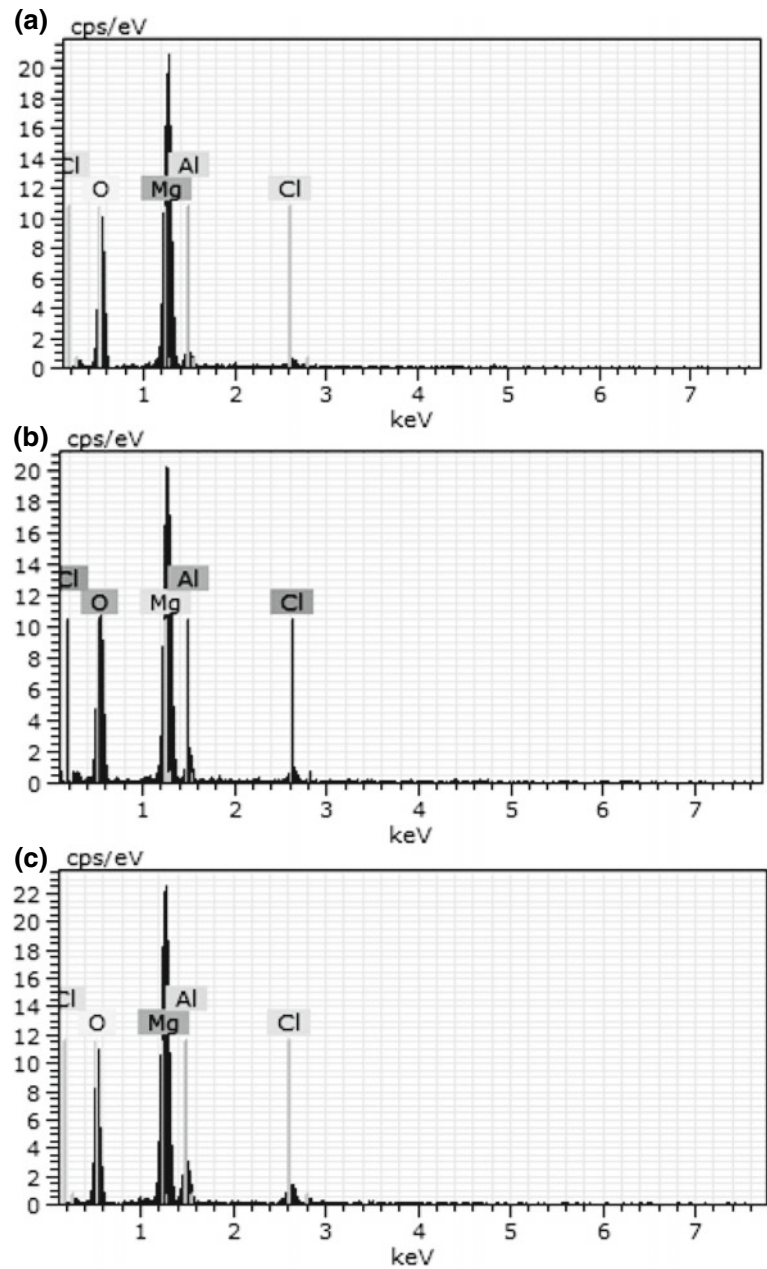
It is known that galvanic corrosion is the primary prospect when active magnesium is coupled with a relatively noble material [12]. But, no galvanic interaction between the alloy matrix and reinforcing fibers and particles could take place since the Al_2O_3 fibers and particles are an insulator. Hypothetically, it implies that the addition of Al_2O_3 fiber to the AM60 alloy should increase the corrosion resistance of the composite.

The previous corrosion study on pure magnesium was carried out in the same 3.5% NaCl solution [15]. It has found that the grain refinement decreased the corrosion resistance of magnesium, which was attributed to the higher density of grain boundaries and other defects from the grain refinement. However, in the case of fiber-reinforced composite, the high density of grain boundaries might not be the main mechanism of decreasing corrosion resistance. The changes in the grain boundary precipitation might appear to be another reason for the reduction in corrosion resistance for the composites. The existence of noble precipitates such as $\text{Mg}_{17}\text{Al}_{12}$ phases at the grain boundaries makes the grain boundaries more corrosion resistant than the matrix and

increases the overall corrosion resistance of the material [7]. In the 7FC and MHNC-7F3NP composites, the lack of such relatively more noble precipitates at the grain boundaries could result in a low corrosion resistance.

The introduction of the fibers and particles in the 7FC and MHNC-7F3NP composites generated new interfaces between the matrix alloy and reinforcements. As both the fibers and particles existed, a large number of new interfaces generated in the composite. As a result, the presence of the new interfaces broke the continuity of the matrix and formed preferential spots for corrosion attack. The poor corrosion resistance of the composites should be attributed to the irregular and less adherent film. No evidence of any localized corrosion or galvanic enhanced corrosion around either the fibres or particles was found. The entire matrix alloy in the composites was uniformly corroded as the remaining fibres and particles stood out of the surface. This type of corrosion was observed in $\text{SiC}_p/\text{ZC71}$ composites by Nunez-lopez et al. [16]. For their practical applications in corrosive environment, the developed composites need to be treated for surface protection, of which investigation proceeds.

Fig. 5 EDS spectra identifying oxygen and chlorine for the **a** unreinforced alloy AM60, and **b** 7FC and **c** MHNC-7F3NP composites, respectively, which corresponds the SEM graphs in Fig. 4



Conclusions

1. The results of the electrochemical tests indicate that the unreinforced as-cast base magnesium alloy AM60 exhibited corrosion resistance higher than its composites, and the reinforcement of the micron-sized Al_2O_3 fibers and/or nano-sized Al_2O_3 particles deteriorated the corrosion resistance of the 7FC and MHNC-7F3NP composites. The addition of the micron-sized fibres at 7 vol.% as reinforcement significantly reduced the corrosion resistance of the matrix alloy AM60 from 4.07 to 2.08 $\text{k}\Omega \text{cm}^2$ by almost 50%. The presence of the nano-sized particles resulted in a reduction of the corrosion resistance of the 7FC composite from 2.08 to 1.88 $\text{k}\Omega \text{cm}^2$ by 0.20 $\text{k}\Omega \text{cm}^2$. This observation indicated that the introduction of the nano-sized particles up to 3 vol.% had almost no effect on the corrosion resistance of the FC composite.
2. The formation of the surface morphology on the corroded unreinforced alloy AM60 resulted from a combined effect of galvanic corrosion, and pitting corrosion. The presence of different phases in the microstructure of the unreinforced alloy AM60 should be responsible for these types of corrosion mechanisms.

3. No galvanic interaction between the alloy matrix and reinforcing fibers and particles could take place since the Al_2O_3 fibers and particles are an insulator. In the composites, the lack of such relatively more noble precipitates such as $\beta\text{-Mg}_{17}\text{Al}_{12}$ phases and Al–Mn intermetallics at the grain boundaries could result in a low corrosion resistance, although the high density of grain boundaries might not be the main mechanism of decreasing in corrosion resistance.
4. The introduction of the fibers and particles in the 7FC and MHNC-7F3NP composites generated new interfaces between the matrix alloy and reinforcements, which broke the continuity of the matrix and formed preferential spots for corrosion attack. The poor corrosion resistance of the composites should be attributed to the irregular and less adherent film on their surface.

Acknowledgements The authors would like to thank the Natural Sciences and Engineering Research Council of Canada, and University of Windsor for supporting this work.

References

1. Zhang Q, Hu H, Lo J (2011) Solidification of discontinuous Al_2O_3 fiber reinforced magnesium (AM60) matrix composite. *Defect and Diffusion Forum.* 312–315: 277–282
2. Banerji A, Hu H, Alpas AT (2012) Ultra-mild wear of Al_2O_3 fibre and particle reinforced magnesium matrix composites. *Adv. Mat. Res.* 445: 503–508
3. Banerji A, Hu H, Alpas AT (2013) Sliding wear mechanisms of magnesium composites AM60 reinforced with Al_2O_3 fibers under ultra-mild wear conditions. *Wear.* 301: 626–635
4. Zhang X, Fang L, Zhang Q, Hu H, Nie X (2014) Fabrication and tensile properties of Al_2O_3 particle and fibre hybrid magnesium-based composites. *J. Chin. Ceramic Soc.* 1(2): 122–128
5. Zhang X, Fang L, Xiong B, Hu H (2015) Microstructure and tensile properties of Mg(AM60)/ Al_2O_3 metal matrix composites with varying volume fractions of fiber reinforcement. *J. Mater. Eng. Perform.* 24(12): 4601–4611
6. Zhang X, Zhang Q, Hu H (2014) Tensile behavior and microstructure of magnesium AM60-based hybrid composite containing Al_2O_3 fibres and particles. *Mat. Sci. Eng. A.* 607: 269–276
7. Mondal AK, Blawert C, Kumar S (2015) Corrosion behaviour of creep-resistant AE42 magnesium alloy-based hybrid composites developed for powertrain applications. *Materials and Corrosion.* 66 (10), 1150–1158
8. Zhou J, Ren L, Geng X, Fang L, Hu H (2017) As-cast magnesium AM60-based hybrid nanocomposite containing alumina fibres and nanoparticles: Microstructure and tensile behavior. *Materials Science & Engineering A.* <https://doi.org/10.1016/j.msea.2017.10.070>.
9. Revie RW (ed) (2000) *Uhlig's Corrosion Handbook*. 2nd ed, John Wiley & Sons, New York
10. Shi Z, Atrens A (2011) An innovative specimen configuration for the study of Mg Corrosion. *Corrosion Science.* 53:226–246.
11. Shi Z, Liu M, Atrens A (2010) Measurement of the corrosion rate of magnesium alloys using Tafel extrapolation. *Corrosion Science.* 52:579–588
12. Bakkar A, Neubert V (2007) Corrosion characterisation of alumina–magnesium metal matrix composites. *Corrosion science.* 49(3):1110–1130
13. Bakkar A, Neubert V (2009) Corrosion behaviour of carbon fibres/magnesium metal matrix composite and electrochemical response of its constituents. *Electrochimica Acta,* 54(5):1597–1606
14. Song GL, Atrens A (1999) Corrosion mechanisms of magnesium alloys. *Adv. Eng. Mater.* 1(1):11–33
15. Ghali E (ed) (2010) *Corrosion resistance of aluminum and magnesium alloy: Understanding, Performance, and Testing.* Wiley, New York
16. Nunez-lopez CA, Skeldon P, Thomson GE, Lyon P, Karimzadeh H, Wilks TE (1995) The corrosion behaviour of Mg alloy ZC71/SiCp metal matrix composites. *Corrosion Science.* 37 (5):689–708